Journal of Sound and Vibration (1999) **226**(5), 923–940
Article No. jsvi.1999.2240, available online at http://www.idealibrary.com on IDEAL®

DYNAMICAL BEHAVIOUR OF THE PLANAR NON-LINEAR MECHANICAL SYSTEM — PART I: THEORETICAL MODELLING

N. JAKŠIĆ, M. BOLTEŽAR, I. SIMONOVSKI AND A. KUHELJ

University of Ljubljana, Faculty of Mechanical Engineering, Aškerčeva 6, 1000 *Ljubljana, Slovenia*

(*Received* 21 *August* 1998, *and in final form* 16 *March* 1999)

A non-linear planar centrifugally excited oscillatory system was studied in its steady-state domain. The dynamic behaviour in phase space was analysed by a model based on the numerical integration of non-linear equations of motion. The integral of the correlation dimension and Lyapunov exponents were used as a quantitative measure to describe the motion of the model. The estimates of the correlation dimension for the values in real phase space and for those obtained by embedding numerical time histories show good agreement. In addition, the visualization procedure, as a qualitative measure, shows good agreement with the results of Lyapunov exponents and the correlation dimension of the model. Power spectral and bispectral analyses have further been used to analyze the behaviour of the model in the frequency domain. The dominance of the first mode was found, while other modes have significantly lower power. In the calculated bicoherences a "wall" of values can be seen, which is attributed to the bicoherence's estimated sensitivity to the division by small number. This sensitivity resulted with an increase in the number of bicoherence peaks. A new approach to reduce the number of divisions by small number is proposed and its advantage over those found in the literature is given.

1. INTRODUCTION

The modelling of non-linear dynamics has been attracting increasing attention in recent years. Modern analytical tools—specifically the analyses in the phase space developed primarily in the basic scientific disciplines—are now entering into the applied technical sciences [1–11]. On the other hand, bispectral analysis is a part of the rapidly expanding field of Higher Order Statistics and can provide information on the quadratic-type non-linearities in the signal. The two parts of this paper endeavour to combine both approaches, using them firstly on a theoretical model and secondly on real technical application.

Dry friction frequently occurs in real technical systems. Its impact on the dynamics of the single-degree-of-freedom (d.o.f.) system is shown in references [1, 3, 4, 12, 13] and on systems with several d.o.f. in references [2, 5, 8–10, 14]. The

0022-460X/99/400923 + 18 $30.00/0

possibility of using the integral of correlation dimension (ICD) as a mean of quantitative phase space analysis to interpret aperiodic time series of the system with dry friction has been shown in reference [2]. Comparisons of the correlation dimension between the real and reconstructed phase space of the mechanical model with several d.o.f. have been given in references [5, 8, 10].

Lyapunov exponents represent another measure for estimating the divergence of trajectories in phase space. They have been used to detect the chaotic behaviour in single [1] and in several [2, 10] d.o.f. models.

The statistical stability of the bispectrum estimate is achieved by dividing the time series into the segments for averaging. Because the variance of the bispectrum estimate is dependent upon the second order properties [15–17], the bispectrum is normalized into the skewness function [15] or bicoherence [18]. When normalizing, attention should be paid to the problem of division by small numbers. One way of dealing with this problem is to add a low-level white Gaussian noise to the signal [18]. In this paper, both the numerator and the denominator of the bicoherence estimate are compared to the numerical threshold for zero value, thus allowing for a check on the possibility of dividing by small number.

In the experimentation, a washing machine was used as the application from the real engineering world. The washing machine's suspension optimization was conducted [14] on the washing complex modelled as a rigid body with 6 d.o.f. The aims were orientated towards several directions. Firstly, it was desired to apply some modern analyses from the non-linear dynamical systems. In the literature, it is seldom found that the dynamics is simultaneously studied in both the real and the reconstructed phase spaces. In addition, an experiment was conducted which enabled estimations to be made of the same measures as in the theoretical modelling, and also in a pair of measured time histories. Secondly, the estimation of bicoherences serves as an additional mean when deciding how to model the system, simultaneously to the phase space estimation.

Finally, the intention was to compare the results of the theoretical modelling of the washing machine's washing complex dynamics, as described in Part I of this paper, with the measured responses in the time, frequency and phase-space domains as described in Part II.

2. DESCRIPTION OF THE MODEL

The model (see Figure 1) consists of two rigid bodies. The first rigid body, with its centre of gravity at point T, is called the basic body. Its links to the surroundings consist of a bilinear spring support, linear viscous damper and element with implemented dry friction. All of the elements of vibroisolation are collinear with the axis of the co-ordinate system $X-Y$. The second rigid body, with its centre of gravity at point T_e, is called the rotor. It is driven by torque $M(t)$ and attached to the basic body by bearings at point S.

The model has four degrees of freedom. Co-ordinates x, y and φ are needed to determine the motion of the basic body. The x and y describe the horizontal and

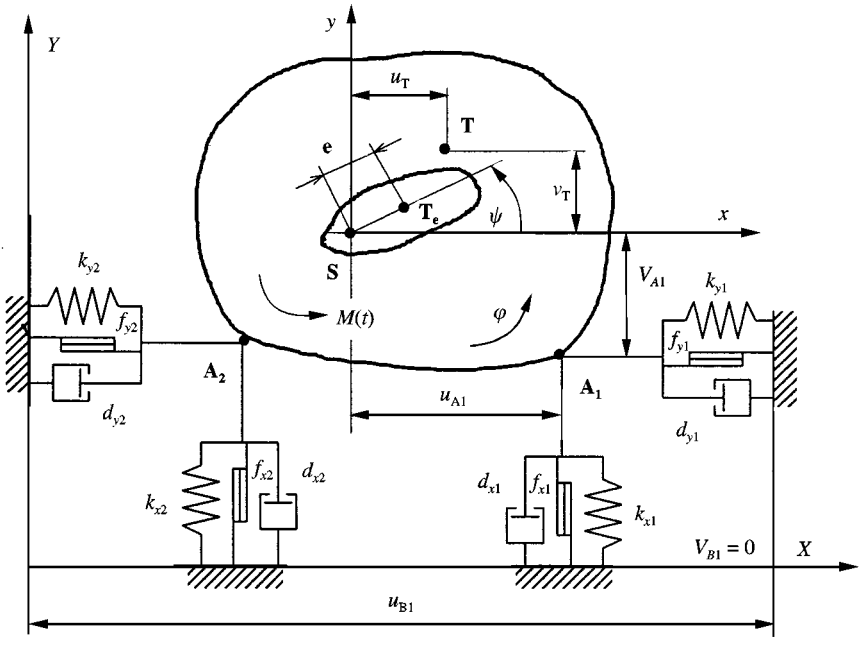

Figure 1. The model.

vertical translation of the basic body, respectively, and φ describes its rotation. To characterize the rotation of the rotor the additional co-ordinate ψ is used. The φ and the ψ start at X-axis. In order to obtain equations of motion, the Lagrangian equations of second order were used; the motion takes place in configuration space, hence $q_1 = x$, $q_2 = y$, $q_3 = \varphi$, $q_4 = \psi$ and so

$$\frac{\mathrm{d}}{\mathrm{dt}} \frac{\partial T}{\partial \dot{q}_j} - \frac{\partial T}{\partial q_j} = Q_j - \frac{\partial V}{\partial q_j}, \quad j = 1, \ldots, 4, \tag{1}$$

where T denotes the kinetic energy, V the potential energy and Q_j are generalized non-conservative forces. The definitions of the functions used are

$$\begin{aligned} h_{xi} &= u_{Ai} \cos\varphi - v_{Ai} \sin\varphi, \qquad h_{yi} = v_{Ai} \cos\varphi + u_{Ai} \sin\varphi, \\ t_x &= u_T \cos\varphi - v_T \sin\varphi, \qquad t_y = v_T \cos\varphi + u_T \sin\varphi, \end{aligned} \tag{2}$$

where the u's and v's are depicted in Figure 1. The kinetic energy of the system can be written as

$$T = \frac{1}{2} J_T \dot{\varphi}^2 + \frac{1}{2} J_{Te} \dot{\psi}^2 + \frac{m}{2} [\dot{x}^2 + \dot{y}^2 + (u_T^2 + v_T^2)\dot{\varphi}^2 + 2\dot{\varphi}(t_x \dot{y} - t_y \dot{x})]$$

$$+ \frac{m_e}{2} [\dot{x}^2 + \dot{y}^2 + e^2 \dot{\psi}^2 + 2e\dot{\psi}(\dot{y} \cos\psi - \dot{x} \sin\psi)], \tag{3}$$

and the potential energy as

$$V = mg(y + t_y) + m_e g(y + e\sin\psi) + \frac{1}{2}\sum_{i=1}^{2} k_{xi}(L_{xoi} - L_{xi})^2 + \frac{1}{2}\sum_{i=1}^{2} k_{yi}(L_{yoi} - L_{yi})^2, \tag{4}$$

where L_{xoi} and L_{yoi} are the undeformed lengths of the springs in the X and Y directions as denoted by their indices, and L_{xi} and L_{yi} are deformed lengths of the same springs at time t:

$$L_{xi} = \begin{cases} L_{xoi}, & L_{xi} \geqslant L_{xoi} \\ |u_{Bi} - x - h_{xi}|, & L_{xi} < L_{xoi} \end{cases}, \qquad L_{yi} = \begin{cases} L_{yoi}, & L_{yi} \geqslant L_{yoi} \\ |v_{Bi} - y - h_{yi}|, & L_{yi} < L_{yoi} \end{cases}. \tag{5}$$

The generalized non-conservative forces consist of the driving torque, friction forces and viscous damping forces. The torque is given by

$$M(t) = a\psi^b, \quad a > 0, \quad b < 0, \tag{6}$$

and represents the driving force of the model, reflecting the real characteristics of the electromotor. The friction forces are given according to the discontinuous Coulomb model of dry friction as

$$F = N\mu_k \operatorname{sgn}(v), \tag{7}$$

where N denotes normal force on the surface, F the friction force, v the relative velocity between surfaces in contact, and μ_k the kinetic coefficient of friction. The excitation is modelled as non-ideal and not explicitly time dependent; hence the model is autonomous.

The parameter identification was done mostly by experimentation and is described precisely in reference [8]. Hence, the parameters of the vibroisolation were determined experimentally in both horizontal and vertical directions. Consequently, the chosen configuration of the suspension simply follows the experimental approach. The details of the model's parameters can be found in Table 1.

3. THE RESULTS OF NUMERICAL SIMULATION

The set of four equations of motion (1) was transformed into a system of eight ordinary differential equations of first order. The numerical integration of the latter was carried out with the Runge–Kutta method with error estimation of $O(h^5)$, where h denotes the constant integration step. The numerical integration always starts at the same initial conditions, which are defined by stable static equilibrium and zero velocities . For a certain set of geometrical and material parameters of the

TABLE 1

The parameters of the model

Rotor	m_e	6·2	kg	Vibroisolation	k_{x1}	7484·591	N/m
	J_{T_e}	0·1939	kg m^2		k_{x2}	14969·182	N/m
	e	0·01719	m		k_{y1}	9701·845	N/m
Basic body	m_t	42·805	kg		k_{y2}	10990·797	N/m
	J_T	2·6811	kg m^2		d_{x1}	79·3	N s/m
	u_t	−0·00854	m		d_{x2}	79·3	N s/m
	v_t	0·04387	m		d_{y1}	107·5	N s/m
	u_{A1}	0·239	m		d_{y2}	107·5	N s/m
	v_{A1}	−0·166	m		N_{x1}	12·222	N
	u_{A2}	−0·239	m		N_{x2}	15·959	N
	v_{A2}	−0·166	m		N_{y1}	116·281	N
Torque	a	119623·5	—		N_{y2}	151·837	N
	b	−2·45023	—		μ_k	1	—

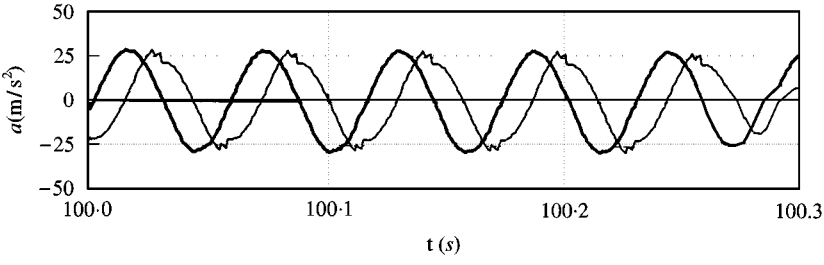

Figure 2. Numerically integrated time histories of accelerations; a_x (——) is horizontal and a_y (——) vertical acceleration.

model, the time histories of accelerations in horizontal (x) and vertical (y) directions are presented in Figure 2. The time histories of integrated accelerations show that the motion of the model has one dominant frequency; hence the frequency of spin dry. The signals of accelerations in horizontal and vertical direction are shifted by $\pi/2$; hence the model's response follows the centrifugal excitation.

3.1. SPECTRAL ANALYSIS

Upon assuming that $x(n)$, $n = 0, \pm 1, \pm 2, \ldots$, is a real, stationary and random process, the discrete third order cumulant spectrum or bispectrum $B(2\pi f_1, 2\pi f_2)$ of $x(n)$ is defined as [19]

$$B(2\pi f_1, 2\pi f_2) = \sum_{\tau_1=-\infty}^{\tau_1=+\infty} \sum_{\tau_2=-\infty}^{\tau_2=+\infty} c_3(\tau_1, \tau_2) \mathrm{e}^{-\mathrm{j}(2\pi f_1 \cdot \tau_1 + 2\pi f_2 \cdot \tau_2)}, \tag{8}$$

where $c_3(\tau_1, \tau_2)$ is the third order cumulant of $x(n)$. The alternative approach is to construct a consistent bispectrum estimate $\hat{B}$ by using the DFT $X(k)$ of a signal $x(n)$, $n = 0, 1, \ldots, N-1$ [15]. When using this technique, the signal of length N points is subdivided into K segments having M points ($N = K \cdot M$). The DFT of each segment is calculated and averaged over K segments:

$$\hat{B}(k_1, k_2) = \frac{1}{K} \sum_{i=0}^{i=K-1} X_i(k_1) X_i(k_2) X_i^*(k_1 + k_2). \tag{9}$$

Here k_1 and k_2 denote the indices of frequency, i is the index of the segment and X^* is the complex conjugate of X. If the highest frequency component f_{max} of the process $x(n)$ complies with Nyquist's sampling condition ($f_{max} \leqslant f_N = f_s/2 = 1/2\Delta t$)), the principal domain of $B(2\pi f_1, 2\pi f_2)$ is composed of inner (IT) and outer (OT) triangles [20]; see Figure 3.

The variance of the bispectrum estimate for stochastic processes can be estimated by using the expression [15]

$$\mathrm{var}\{\hat{B}(k_1, k_2)\} \propto MP(k_1)P(k_2)P(k_1 + k_2), \tag{10}$$

where P denotes the power spectrum. The bispectrum estimate is therefore sensitive to both second and third properties. To eliminate the sensitivity of the bispectrum estimate to second order properties, a new measure called the skewness function was introduced [15]. However, for the bispectra of signals, conforming to the cosine model [16, 18],

$$x(n\,\Delta t) = \sum_i A_i \cos(2\pi f_i\, n\,\Delta t + \phi_i) + noise_{Gauss}(n), \tag{11}$$

an alternative normalization called bicoherence is often used [17, 21]:

$$\hat{b}^2(k_1, k_2) = \frac{|\hat{B}(k_1, k_2)|^2}{(1/K)\sum_{i=0}^{i=K-1} |X_i(k_1)X_i(k_2)|^2 \hat{P}(k_1 + k_2)}. \tag{12}$$

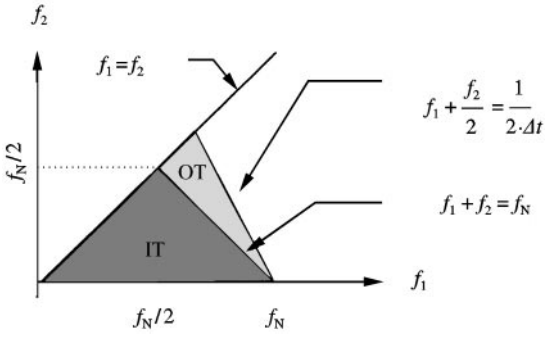

Figure 3. The principal domain of the discrete bispectrum.

In equation (11), A_i and ϕ_i denote random amplitude and random phase, generated at the beginning of each segment, and f_i denotes the frequency of the ith mode.

One useful property of the bicoherence is that it is bounded between zero and unity, a property which the skewness function does not share. The bicoherence $\hat{b}(k_1, k_2)$ can be interpreted as a portion of power due to the quadratic phase coupling (QPC) of frequency components k_1 and k_2 [17]; thus when QPC takes place bicoherence should be close to unity. To distinguish between low, but non-zero, bicoherence values and truly zero bicoherence values, the minimal significant value of the bicoherence must be calculated,

$$\hat{b}^2_{sig.} = -\frac{\ln(1 - T_{\alpha\%})}{K}, \tag{13}$$

where $T_{\alpha\%}$ is the significance in %. The $\hat{b}^2_{sig.}$ is based on the assumption that the process involved is Gaussian, in which case the bicoherence should be approximately χ^2 distributed with two degrees of freedom [22].

When dealing with signals conforming to the sinusoidal model, the assumption of phase randomization between various sinusoidal components is assumed. If the phases of the various sinusoidal components are constant for all segments, bicoherence can peak even if no QPC takes place [18]. To overcome this problem Fackrell proposed testing the phase of the bispectrum. It was shown [18] that in the case of QPC, the phase of the bispectrum is zero. If the phase of the bispectrum is approximately normally distributed around the true phase [21], the maximal phase for a given significance level $T_{\theta\%}$ can be determined. The $T_{\theta\%}$ is determined from the standard normal tables $N(\mu, \sigma)$, where μ denotes mean value and σ a standard deviation:

$$\theta_{sig.}(k_1, k_2) = \frac{T_{\theta\%}}{\sqrt{2K}} \sqrt{1\hat{b}^2(k_1, k_2) - 1}. \tag{14}$$

Thus, only the bicoherence values greater than equation (13) and lower than equation (14) are considered for QPC detection.

The power spectra were calculated by using 4096 FFT points per segment. Overlapping of 5% was used to obtain 128 segments and the Hamming window was applied in the time domain. The power spectra of horizontal and vertical acceleration are presented in Figures 4 and 5. In the horizontal direction the spin dry frequency of 17·57 Hz is clearly visible. All other frequencies contain significantly lower power. In the vertical direction, Figure 5, the spin dry frequency of 17·57 Hz and its higher harmonics at 52·73 Hz (3×) and 87·4 Hz (5×) can be extracted. All other frequencies have a power lower than -70 dB. It is interesting to note that only odd harmonics appear. This is due to the fact that the signal meets the requirement of symmetry of the third kind in Fourier analysis.

The bicoherences of horizontal and vertical accelerations were calculated using 1024 FFT points per segment, giving a frequency resolution of 1·95 Hz. Overlapping of 5% was used to obtain 513 segments for averaging. Because of its ability to resolve QPC peaks [18, 23] the Hamming window was applied in the

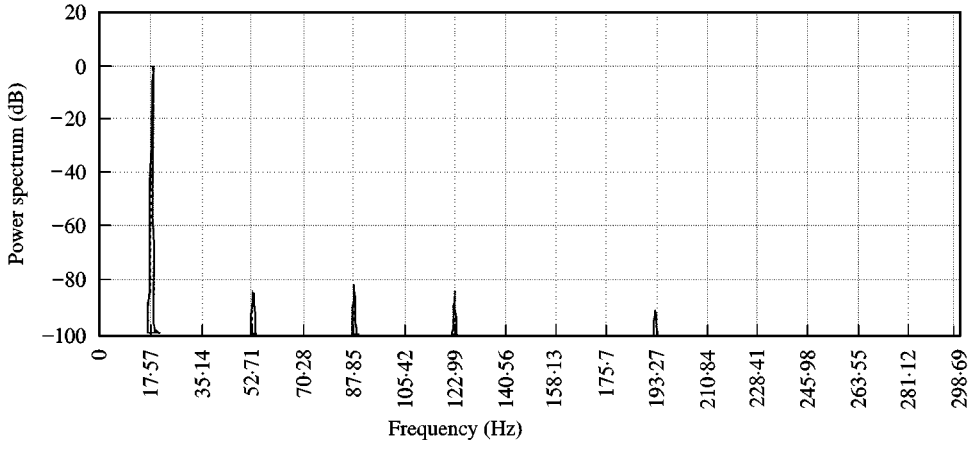

Figure 4. Power spectrum of horizontal model's acceleration.

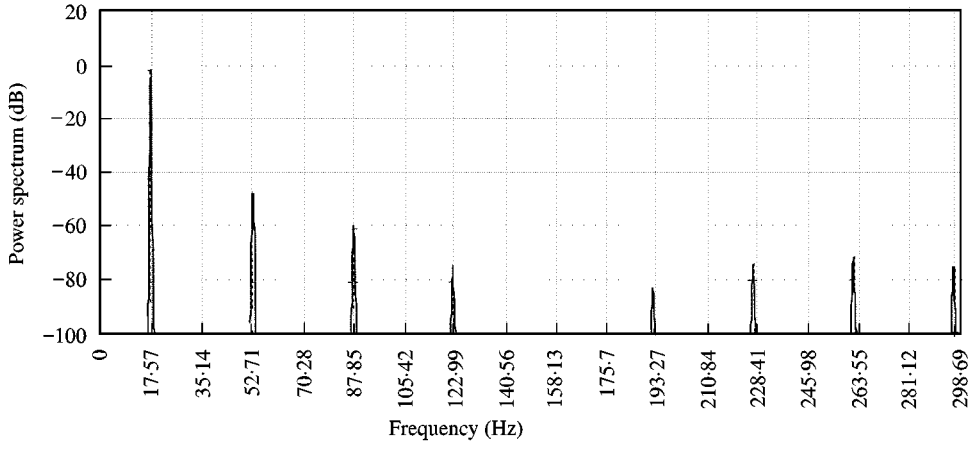

Figure 5. Power spectrum of vertical model's acceleration.

time domain. The number of segments and the selected significance level of $T_{\alpha\%} = 95\%$ defined the minimal significant bicoherence value of 0·0058. The significance level of $T_{\theta\%} = 95\%$ was used to determine the maximal allowed phase of the bispectrum. The bicoherences of horizontal and vertical acceleration are presented in Figures 6 and 7. In both figures, a "wall" of bicoherence values $\approx 0{\cdot}35$, $\approx 0{\cdot}23$ is clearly visible. This is the result of the normalizing process. When normalizing, the bispectrum is divided by the power spectrum and by another factor; see equation (12). When the denominator is small, the problem of the division by a small number occurs and can result in high bicoherence values. Because of the division, the bicoherence can peak even if the numerator is very small or close to zero. One must bear in mind that the bicoherence gives the proportion of the power due to the QPC of components k_1 and k_2, irrespective of the power of these two components. If there is a large amount of QPC between

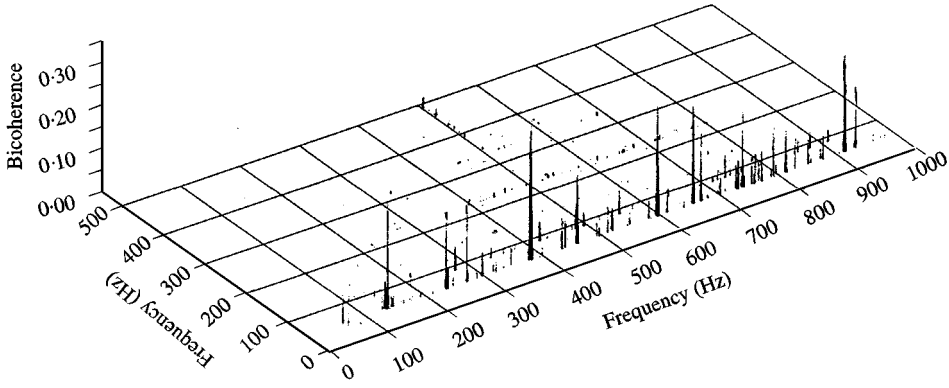

Figure 6. Bicoherence surface plot of horizontal model's acceleration.

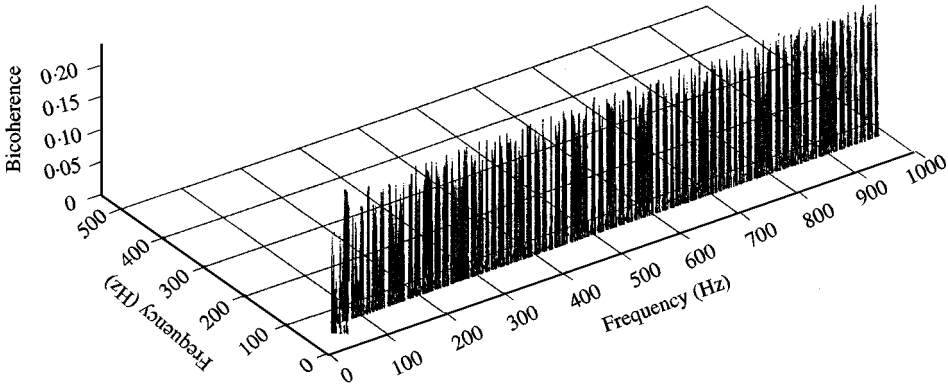

Figure 7. Bicoherence surface plot of vertical model's acceleration.

frequencies with small power, the QPC between frequencies with high power would be among the large number of high bicoherence values. In other words, no matter how small may be the power of components k_1 and k_2, if the phases of these two components quadratically couple, the bicoherence exhibits a peak. The question is: should the bicoherence peak if the power of the components k_1 and k_2 is significantly lower than the power of the largest components? If the power spectrum is composed of several distinct high values and has virtually no power elsewhere, the problem of the division by small number can occur even more often. One way of tackling this problem is to add low-level white Gaussian noise to the signal [18]. This ensures that there is always some power in the spectral component at each frequency, and so even if the bispectrum is zero, the denominator is always greater than zero. The drawback of this approach is that it reduces the bicoherence values.

In this paper an alternative approach to determining the numerical threshold for zero value has been implemented. Whenever the numerator is smaller than this threshold the bicoherence is set to zero. If the numerator is greater, and the

denominator smaller than this threshold, a small, constant and positive value is added to the denominator. By increasing the numerical threshold the number of divisions by small number is decreased. However, it is difficult to determine when to stop increasing the numerical threshold.

In order to compare both approaches, the bicoherence of the vertical accelerations has been estimated twice: first on a signal with added Gaussian noise with zero mean value and 0·5 variance, … SNR = 29 dB (called case a), and second on a signal without added Gaussian noise but with 1E-10 as a numerical threshold for zero value (called case b). The numerical threshold of 1E-10 is 182 dB smaller than the maximum value of the magnitude bispectrum of the vertical accelerations with no noise added; see Table 2. The case a, the number of the peaks in the wall decreased as did the values of the bicoherence. The "wall" however remained; see Figure 8. Applying only numerical threshold for zero value of 1E-10, case b, resulted in a great reduction in the number of bicoherence peaks: the "wall" could hardly be distinguished, while the highest bicoherence value only slightly decreased ($\approx 0{\cdot}22$); compare Figures 7 and 9. Moreover, some of the highest peaks in the bicoherence, see Table 3, were at the same frequency as the peak of the magnitude bispectrum, see Table 2. The effectiveness of the approach is clearly evident.

The magnitude bispectra of both horizontal and vertical accelerations have also been calculated. For both accelerations only QPC at (17·57, 17·57) Hz were

TABLE 2

Magnitude bispectrum values for horizontal and vertical accelerations of the model

Horizontal accelerations	Vertical accelerations
0·21 at (17·57, 17·57) (Hz)	0·13 at (17·57, 17·57) (Hz)

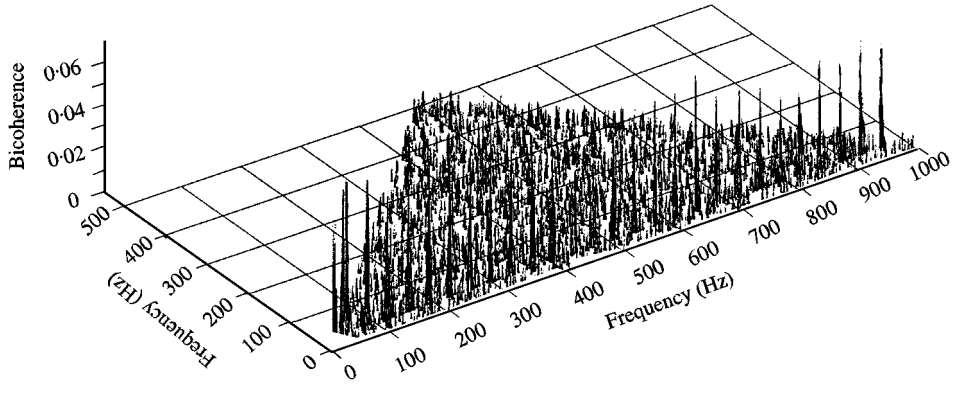

Figure 8. Bicoherence surface plot of vertical model's acceleration. Gaussian noise with zero mean value and variance 0·5 was added to the signal.

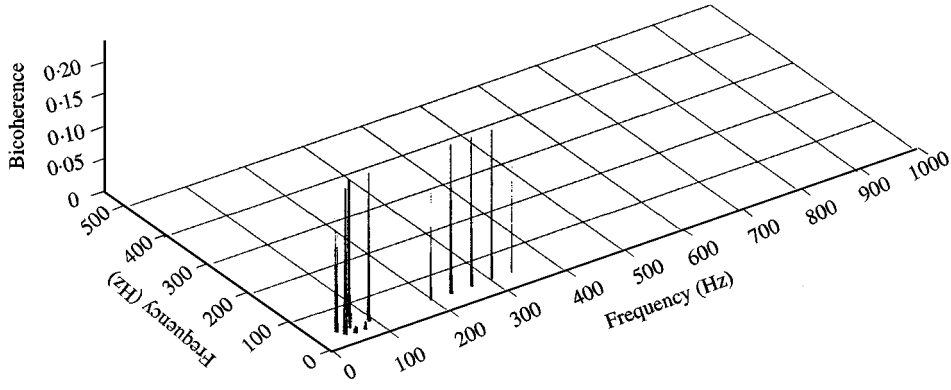

Figure 9. Bicoherence surface plot of vertical acceleration-model. No added Gaussian noise. Numerical threshold for zero value was 1E-10.

TABLE 3

Bicoherence values of vertical model's accelerations. Numerical threshold for zero value 1*E*-10

Frequency (Hz)	(17·57, 17·57)	(52·73, 35·17)	(87·89, 35·17)	(332·03, 35·17)
Bicoherence	0·221	0·221	0·221	0·222

found; see Table 2. Thus, the QPC of the basic harmonic partly generates second harmonics, the power of which is here negligible; see Figures 4 and 5.

The magnitude bispectra were calculated because it has been found useful to check magnitude bispectrum for QPC [23] when the number of bicoherence peaks is large. This is due to the fact that no division is needed to calculate the bispectrum, thus eliminating the problem of division by a small number. However, the statistical stability of the bispectrum estimate requires that the bispectrum's number of degrees of freedom be larger than 120 [18, 23].

3.2. PHASE-SPACE ANALYSIS

Although the integration of the full set of equations of motion allows one to create the real phase space, interest here lies also in the reconstruction process [24, 25] on the basis of a single numerically integrated time history of the system's dynamics. From a single measured time history $q(t)$, one can create delay vectors

$$\mathbf{X}(t) = \{q(t), q(t-\tau), \ldots, q(t-(d-1)\tau)\}, \tag{15}$$

where τ is the delay time and d is the embedding dimension. In order to find the appropriate delay time for the embedding procedure, the autocorrelation function

of the time history $q(t)$ was calculated and for the value of τ the first decorrelation time was taken into account.

3.2.1. *Correlation dimension*

To characterize the dimensionality of an attractor in real as well as in reconstructed phase space, the integral of correlation dimension (ICD) was estimated. It is defined as [26, 27]

$$ICD(N, L) = \frac{2}{N(N-1)} \sum_{i=1}^{N-1} \sum_{j=i+1}^{N} \mathrm{H}(L - \| \mathbf{X}_i - \mathbf{X}_j \|), \tag{16}$$

where N denotes the number of points of the phase space, H is the Heaviside function, L the characteristical length and $\| \mathbf{X}_i - \mathbf{X}_j \|$ denotes the distance between two points $\mathbf{X}_i$ and $\mathbf{X}_j$ of the phase space. This distance can be defined as

$$\| \mathbf{X}_i - \mathbf{X}_j \| = \max |(\mathbf{X}_i)_k - (\mathbf{X}_j)_k|, \quad k = 1, \ldots, d. \tag{17}$$

It has been shown [26, 27] that for most chaotic attractors and for small L-s ICD scales like

$$ICD(N, L) \propto L^{\nu}, \tag{18}$$

where ν denotes the correlation dimension of the attractor in d-dimensional phase space.

The extraction of the correlation dimension in the real phase space of the model resulted in an estimate for the correlation dimension where $\nu = 1{\cdot}00 \pm 0{\cdot}00$; see Figure 10. It was then possible to compute the integrals of correlation dimension after forming delay vectors from a single numerically integrated time history. For

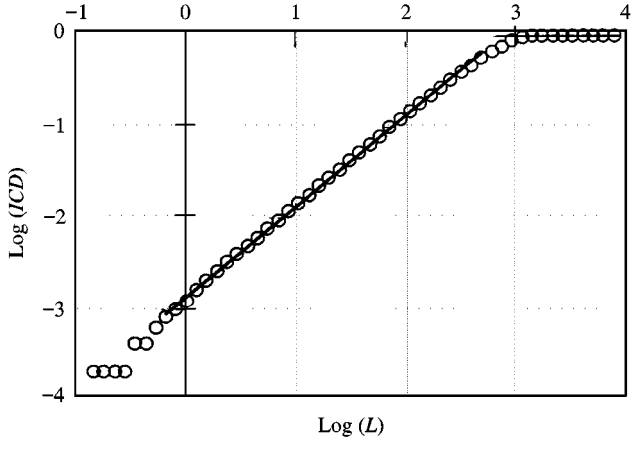

Figure 10. Integral of correlation dimension, real phase space of the model.

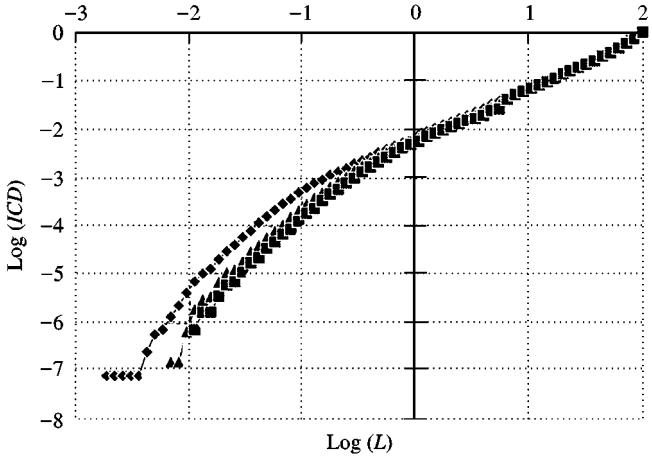

Figure 11. Integral of correlation dimension, reconstructed phase space on vertical acceleration of the model. d values: —◆— 3; —▲— 9; —■— 15.

TABLE 4

Estimation of the correlation dimension of the model based on different numerically integrated time histories

v	Displacement	Velocity	Acceleration
Horizontal direction	1·15 ± 0·01	1·03 ± 0·00	1·04 ± 0·00
Vertical direction	1·09 ± 0·01	1·03 ± 0·00	1·06 ± 0·01

vertical acceleration, the integrals of correlation dimension for the three embedding dimensions are shown in Figure 11. The values of the correlation dimension estimates for the different time histories are shown in Table 4. They differ from 3 to 15% compared with those obtained in real phase space. The most significant difference between real and reconstructed phase space in the correlation dimension estimation is found in horizontal displacement due to decaying transient vibrations visible only in this signal [8]. This results from the inherent property of the driving torque model that was used to model the electromotor characteristics. The driving torque reaches zero value at infinity, and consequently the rotational speed reaches maximum value at infinity. Hence, the model never really reaches the steady state in the very strict theoretical sense, but after some time the growth of velocity becomes negligible from the technical point of view.

In the case of the real phase space, 10,000 points were used; see Figure 10. All of the results in Table 4 and plots in Figure 11 are based on a computation using 5000 points [28] when reconstructing the phase space.

3.2.2. *Lyapunov exponents*

The Lyapunov exponents measure the exponential divergence (positive exponents) or convergence (negative exponents) of two initially neighbouring

trajectories in the phase space; hence the chaotic or regular behaviour of the system under consideration could be detected [24, 29–31]. One can monitor the long-term evolution of infinitesimal n-dimensional sphere of initial conditions in n-dimensional phase space. The sphere will become an n-dimensional ellipsoid. The ith Lyapunov exponent in n-dimensional phase space is defined [31] as

$$\lambda_i = \lim_{t \to \infty} \frac{1}{t} \ln \frac{p_i(t)}{p_i(0)}, \quad i = 1, \ldots, n, \tag{19}$$

where $p_i(t)$ is the length of the ellipsoid principal axis and $p_i(0)$ is the length of the infinitesimal sphere's axis. If at least one of the Lyapunov exponents is greater than zero, then the system exhibits chaotic dynamics.

The technique [31] for computing the complete Lyapunov spectrum of exponents directly from explicitly known equations of motion has been used. The method calculates the Lyapunov spectrum by numerical integration of n non-linear equations of motion for some post-transient initial conditions and the n linearized equations of motion for n different initial conditions that define the arbitrary co-ordinate system defined by n orthonormal base vectors. Because of the exponential divergence of trajectories of the chaotic system, each base vector will diverge in magnitude and tend to fall into a local direction of most rapid growth, the Gram–Schmidt reorthonormalization [31] procedure should be used repeatedly.

The largest Lyapunov exponent was estimated as $\lambda_{max} = -0{\cdot}68$; see Figure 12, hence the model's motion is regular and the model's attractor is a limit cycle.

3.2.3. *Attractor visualization*

The attractor visualization enables one to visualize the attractor's shape in such a way that a trajectory in the phase space is presented in the Euclidean space of the

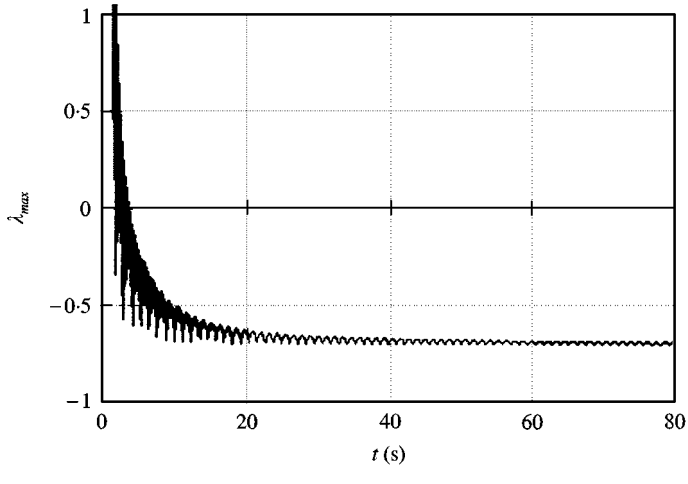

Figure 12. Convergence of the model's largest Lyapunov exponent.

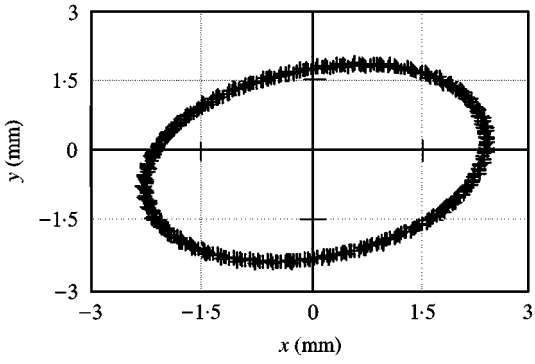

Figure 13. Visualization of the model's plane motion.

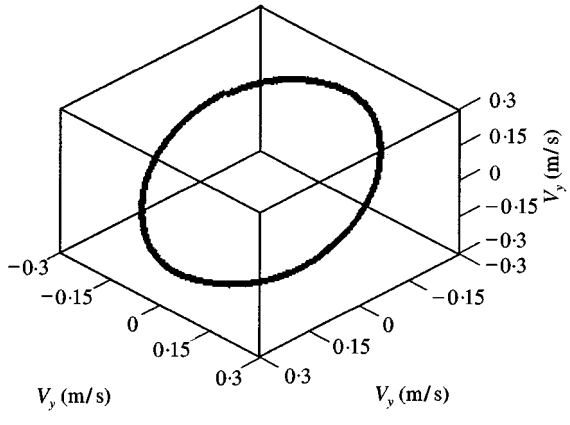

Figure 14. Visualization of the model's attractor reconstructed from the vertical velocity time history.

same dimension. The major drawback of the method is that one is able only to present three-dimensional objects. In the case of multi-dimensional phase space, one could present the attractor's shape in the form of two- or three-dimensional slices of multi-dimensional Euclidean space.

The cross-section of real phase space of the time history of co-ordinates x and y presents an in-plane motion of the model's point S during spin dry; see Figure 13.

The visualized attractor reconstructed from the vertical velocity time history in three-dimensional space, $d = 3$, is shown in Figure 14.

Each of the visualizations suggests that the model's attractor is likely to be the limit cycle.

4. CONCLUSIONS

In this paper the steady state responses, extracted from the non-linear centrifugally excited planar oscillatory system were studied. The work is aimed at finding a better understanding and modelling of non-linear behaviour in machine dynamics.

Concentration has been on the planar model of the washing-machine washing complex due to its negligible motions of the washing complex in the direction perpendicular to the plane of motion.

The computation of the correlation dimension of the real phase space and reconstructed phase space, based on different simulated time histories, has been carried out. The correlation dimension of the model's real phase space and of the reconstructed ones shows good agreement even though the model never really reaches the steady state in the very strict theoretical sense, but after some time the growth of velocity becomes negligible from the technical point of view. This phenomenon is the consequence of the torque model used, and is reflected in the slightly higher estimation of the correlation dimension from the signal of the horizontal displacement due to decaying transient vibration. The estimated values of correlation dimension of the model's attractor point towards the limit cycle as being the attractor's shape.

The estimated negative value of the largest Lyapunov exponent, computed directly from explicitly known equations of motion, is reflected in the model's regular nature of motion.

It is impossible to visualize the complete model's attractor on account of its eight-dimensional phase space. The visualization of the section of the real phase space and the sections of the reconstructed one reveals the attractor as a limit cycle, thus showing good agreement with visualizations of the model's real phase space and of the reconstructed ones.

Each of the phase-space analyses conducted confirms that the model's dynamics is regular and that its attractor is a limit cycle.

The power spectral and bispectral analysis was used next to analyse the dynamical model of the washing complex. The dominance of the first mode has been found, while other modes have significantly lower power values. When calculating bicoherences, attention should be paid to the sensitivity to division by small numbers. This sensitivity can greatly influence the calculated results. In this study, this effect was interpreted as the main reason behind the large number of the bicoherence peaks ("wall"). To overcome this problem other authors have proposed adding Gaussian noise to the signal. However, this resulted in lower bicoherence values.

An alternative approach has been proposed here. A numerical threshold for zero value was introduced, and both numerator and denominator were checked for near zero values. If the numerator was lower than this threshold, bicoherence was set to zero. If the numerator was greater than the threshold, the denominator was checked for the possibility of division by small number. If it was smaller than the threshold, a small positive constant was added. This approach significantly reduced the number of divisions by a small number.

REFERENCES

1. S. Narayanan and K. Jayaraman 1991 *Journal of Sound and Vibration* **146**, 17–31. Chaotic vibration in a non-linear oscillator with Coulomb damping.

2. R. Barron, J. Wojewoda, J. Brindley and T. Kapitaniak 1993 *Journal of Sound and Vibration* **162**, 369–375. Interpretation of aperiodic time series: a new view of dry friction.
3. B. Feeny 1992 *Physica D* **59**, 25–38. A nonsmooth Coulomb friction oscillator.
4. B. Feeny and F. C. Moon 1994 *Journal of Sound and Vibration* **170**, 303–323. Chaos in a forced dry-friction oscillator: experiments and numerical modelling.
5. M. Boltezar N. Jakšić and A. Kuhelj 1996 *EUROMECH—2nd European Non-linear Oscillation Conference*, *Prague*, 9–13 *September*, 97–100. Phase space analysis of the non-linear centrifugally excited planar oscillatory system.
6. D. Logan and J. Mathew 1996 *Mechanical Systems and Signal Processing* **10**, 241–250. Using the correlation dimension for vibration fault diagnosis of rolling element bearings—I. Basic concepts.
7. D. Logan and J. Mathew 1996 *Mechanical Systems and Signal Processing* **10**, 251–264. Using the correlation dimension for vibration fault diagnosis of rolling element bearings—II. Selection of experimental parameters.
8. N. Jakšić 1997 *M.Sc. Thesis*, *Ljubljana*. Vibration analysis of the non-linear centrifugally excited planar system (in Slovene).
9. I. Grabec 1988 *International Journal of Machine Tools and Manufacturing* **28**, 19–32. Chaotic dynamics of the cutting process.
10. M. Boltezar and N. Jakšić 1998 *Zeitschrift für Angewandte Mathematik und Mechanik* **78**, 287–288. Quantitative phase space analysis of the nonlinear planar oscillatory system.
11. M. Boltežar and J. K. Hammond 1999 *Mechanical Systems and Signal Processing* **13** (3), 375–394. Experimental study of the vibrational behaviour of a coupled non-linear mechanical system.
12. S. W. Shaw 1986 *Journal of Sound and Vibration* **108**, 305–325. On the dynamic response of a system with dry friction.
13. J. P. Den Hartog 1931 *Transactions of The ASME* **53**, 107–115. Forced vibrations with combined Coulomb and viscous friction.
14. O. S. Türkay, B. Kiray, A. K. Tuğcu and I. T. Sümer 1995 *Mechanical Systems and Signal Processing* **9**, 359–377, Formulation and implementation of parametric optimisation of a washing machine suspension system.
15. M. J. Hinich 1982 *Journal of Time Series Analysis* **3**, 169–176. Testing for Gaussianity and linearity of a stationary time series.
16. V. Chandran and S. L. Elgar 1992 *IEEE Transactions on Signal Processing* **39**, 2640–2651. Mean and variance estimate of the Bispectrum of a harmonic random process—An analysis including leakage effects.
17. Y. C. Kim and E. J. Powers 1979 *IEEE Transactions on Plasma Science* **PS-7**, 120–131. Digital bispectral analysis and its application to nonlinear wave interactions.
18. J. W. Fackrell 1996 *Ph.D. Thesis*, *The University of Edinburgh*. Bispectral analysis of speech signals.
19. C. H. Nikias and A. P. Petropulu 1993 *Higher-Order Spectra Analysis*, *A Nonlinear Processing Framework*. Englewood Cliffs, NJ: Prentince-Hall.
20. M. J. Hinich and H. Messer 1995 *IEEE Transactions on Signal Processing* **43**, 2130–2134. On the principal domain of the discrete bispectrum of a stationary signal.
21. S. Elgar and G. Sebert 1989 *Journal of Geophysical Research* **94**, 10993–10998. Statistics of bicoherence and biphase.
22. R. A. Haubrich 1965 *Journal of Geophysical Research* **70**, 1415–1427. Earth noise, 5 to 500 Lilicycles per second.
23. I. Simonovski 1998 *M.Sc. Thesis*, *Faculty for Mechanical Engineering*, *University of Ljubljana*. Third order spectra analysis of nonlinear dynamical systems (in Slovene).
24. J. P. Eckmann and D. Ruelle 1985 *Reviews of Modern Physics* **57**, 617–655. Ergodic theory of chaos and strange attractors.

25. F. Takens 1980 *Lecture Notes in Mathematics: Proceedings of Dynamical Systems and Turbulence*, *Warwick*, Vol. 898. Berlin: Springer. Detecting strange attractors in turbulence.
26. P. Grassberger and I. Procaccia 1983 *Physical Review Letters* **50**, 346–349. Characterisation of strange attractors.
27. P. Grassberger and I. Procaccia 1983 *Physica 9D* 189–208. Measuring the strangeness of strange attractors.
28. J. P. Eckmann and D. Ruelle 1992 *Physica D* **56**, 185–187. Fundamental limitations for estimating dimensions and Lyapunov exponents in dynamical systems.
29. U. Parlitz 1991 *International Journal of Bifurcation Chaos* **2**, 155–165. Indentification of true and spurious Lyapunov exponents from time series.
30. M. T. Rosenstein, J. J. Collins and C. J. De Luca 1993 *Physica D* **65**, 117–134. A practical method for calculating largest Lyapunov exponents from small data sets.
31. A. Wolf, J. B. Swift, H. L. Swinney and J. A. Vastano 1985 *Physica* 16*D*, 285–317. Determining Lyapunov exponents from a time series.